Convective Cage Release in Model Colloidal Glasses

Alan R. Jacob,[1] Andreas S. Poulos,[2] Sunhyung Kim,[3] Jan Vermant,[4] and George Petekidis[1,*]
[1]IESL-FORTH & Materials Science & Technology Department, University of Crete, 71110 Heraklion, Greece
[2]Jülich Centre for Neutron Science (JCNS-1) and Institute for Complex Systems (ICS-1), Forschungszentrum Jülich GmbH, 52425 Jülich, Germany
[3]Chemical Engineering Department, Katholieke Universiteit Leuven, Willem de Croylaan 46, 3001 Heverlee, Belgium
[4]Department of Materials, ETH Zürich, Vladmir Prelog weg 5, CH-8093 Zürich, Switzerland
(Received 10 April 2015; revised manuscript received 25 August 2015; published 17 November 2015)

The mechanism of flow in glassy materials is interrogated using mechanical spectroscopy applied to model nearly hard sphere colloidal glasses during flow. Superimposing a small amplitude oscillatory motion orthogonal onto steady shear flow makes it possible to directly evaluate the effect of a steady state flow on the out-of-cage (α) relaxation as well as the in-cage motions. To this end, the crossover frequency deduced from the viscoelastic spectra is used as a direct measure of the inverse microstructural relaxation time, during flow. The latter is found to scale linearly with the rate of deformation. The microscopic mechanism of flow can then be identified as a convective cage release. Further insights are provided when the viscoelastic spectra at different shear rates are shifted to scale the alpha relaxation and produce a strain rate-orthogonal frequency superposition, the colloidal analogue of time temperature superposition in polymers with the flow strength playing the role of temperature. Whereas the scaling works well for the α relaxation, deviations are observed both at low and high frequencies. Brownian dynamics simulations point to the origins of these deviations; at high frequencies these are due to the deformation of the cages which slows down the short-time diffusion, while at low frequency, deviations are most probably caused by some mild hydroclustering.

DOI: 10.1103/PhysRevLett.115.218301 PACS numbers: 82.70.Dd, 64.70.P-, 83.10.Mj, 83.50.-v

The flow of glasses is an intriguing subject in condensed matter physics, both of fundamental interest [1,2] and technological importance, in a variety of systems from polymers and colloids [3] to spin and metallic glasses [4,5]. Colloidal hard spheres (HS) have been used as relevant model systems to investigate both ordered and glassy states [6,7]. The glass transition occurs due to a long-lived entropic caging of a particle when the volume fraction exceeds a critical value of about $\phi = 0.59$ [8–10]. As the long-time, out-of-cage motion (α relaxation) is suppressed, diffusive motion is the only relaxation mode detected at short length and time scales corresponding to in-cage Brownian motion (β relaxation) [3,11]. Such colloidal glasses provide a rigorous testing ground for fundamental problems of flowing nonergodic systems where internal dynamics, nonequilibrium microstructure, and mechanical properties are accessible for direct comparison with computer simulations. Different theoretical approaches based, for example, on mode coupling theory adapted to flowing systems [12] and activated hopping approaches [13], provide insights and challenging predictions.

While the mechanisms of yielding and flow of model hard sphere glasses have been extensively investigated, both for steady [7,14–18] and oscillatory shear flow [19–22] several aspects are still unresolved. Not unimportantly, the mechanism of flow is ill understood. Experiments that aim to investigate this by studying the scaling of shear induced diffusivity with the applied macroscopic shear rate do not reveal a simple flow mechanism and have been the subject of controversy [23,24]. Measurements, where the scaling of nonlinear oscillatory frequency sweeps were used to obtain a strain rate-frequency superposition (SRFS), have been proposed as to elucidate the flow mechanism [25], but so far they have been proven problematic [26], in part due to a complex kinematic history which mixes in with the nonlinear response of the system. In the present work, we use a strategy to explore a wide range of time scales that bears similarities to time temperature superposition (TTS) used in polymeric systems, but with shear used to control the effective temperature in the glass.

Orthogonal superposition rheometry (OSR) combines two deformation modes, steady shear and small amplitude oscillatory shear applied simultaneously and orthogonally to each other. In this way, small amplitude orthogonal frequency sweeps orthogonally interrogate the sample and retrieve its viscoelastic spectra under steady shear [27–33]. Our approach is fundamentally different from SRFS [25] as superposition rheometry is based on the linear measurements of a perturbation spectrum characterizing a strongly nonlinear state; hence, the kinematics of the flow field that create the nonlinear response are simple, and the spectrum can be directly and gently probed. This technique, that now has been made sensitive enough, enables us to probe model colloidal glasses under steady shear without resorting to

nonlinear oscillatory measurements with complicated intracycle kinematics.

In the present work, we directly measure how the flow in glasses proceeds, by measuring how it affects the α and β relaxations in colloidal suspensions of model hard spheres. To this end, we measure the full viscoelastic spectrum of sheared HS glasses through OSR and first determine the characteristic crossover frequency ω_c, which provides a direct measure of the shear induced structural relaxation. Second we use the shear rate evolution of this crossover frequency to investigate if a scaling of the perturbation spectra can be achieved.

We used sterically stabilized poly(methyl methacrylate) (PMMA) nearly hard-sphere particles of 196 nm radius with polydispersity $\sigma \simeq 20\%$, dispersed in an octadecene-bromonaphthalene solvent (refractive index 1.485) to minimize residual van der Waals attractions and evaporation. Volume fractions, initially estimated from random closed packing ($\phi_{\rm rcp} = 0.67$), were precisely determined by matching the magnitudes of the moduli to the master curve provided by Koumakis *et al.* [34]. Superposition rheometry was performed using an ARES-G2 (TA) rheometer with a home modified normal force control loop, equipped with a custom built open bottom double wall Couette geometry [31,33,35]. Steady shear flow was imposed in the tangential direction and the small strain amplitude oscillatory motion was imposed vertically. We investigated steady state shear rates $\dot{\gamma}$ from 10^{-4} to 1 s^{-1} ($\approx 10^{-5}$ to 10^{-1} Pe), represented below by the dimensionless Peclet number, $\mathrm{Pe} = \dot{\gamma} t_B$, where $t_B = R^2/D_0$ ($= 0.158$ s) is the time scale of Brownian motion and D_0 the bare diffusion coefficient. Orthogonal frequency sweeps at a low strain amplitude ($\sim$0.7%) in the linear regime (see Supplemental Material [35]) were performed once steady state shear with $\dot{\gamma}$ was reached. To prevent slip, at low Pe < 1 tools were roughened by coating of similar PMMA particles [36]. Moreover, we largely avoided measurements in the shear banding regime (at very low Pe) [23] except for the highest $\phi = 0.64$ and for $\mathrm{Pe} < 10^{-4}$. Complementarily, we conducted Brownian dynamics (BD) simulations [37] using 50 000 particles with 10% polydispersity and periodic boundary conditions for $\phi = 0.62$ at rest, Pe $= 0.01$ and 0.1 (see Supplemental Material [35]).

Orthogonal superposition experiments were performed at various Pe and three volume fractions, 0.60, 0.61, and 0.64. Figure 1(a) shows frequency sweeps at $\phi = 0.61$, performed at different Pe. At low Pe the data of Fig. 1(a) reveals a response similar to that of a quiescent glass (see Supplemental Material [35]) with $G' > G''$ for all ω 's measured. As Pe is increased flow induces microstructural changes and speeds-up internal dynamics as manifested by the crossover frequency ω_c (at $G' = G''$), entering the experimental window. A scaling of the moduli as a function of frequency for the different steady state shear rates was produced through shift of the data in the x and y axes by factors a and b, respectively, in a way that the crossover

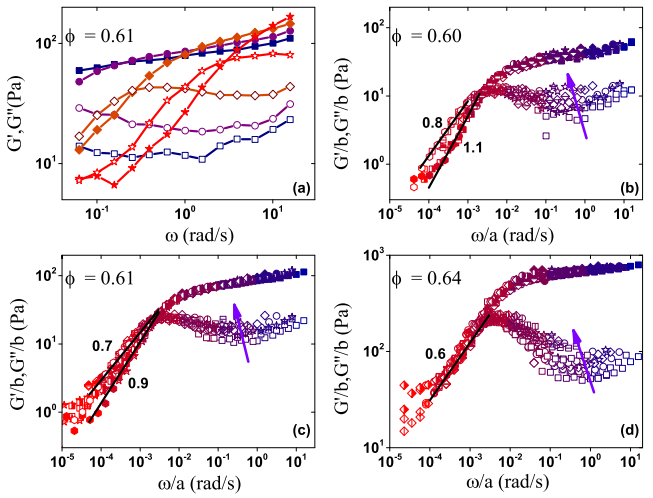

FIG. 1 (color online). (a) The orthogonal frequency sweeps at $\phi = 0.61$ for $\mathrm{Pe} = 2 \times 10^{-1}$ (filled star), 2×10^{-2} (filled diagonal), 2×10^{-3} (filled circle), and 2×10^{-4} (filled square). SROFS data at $\phi = 0.60$ (b), $\phi = 0.61$ (c), and $\phi = 0.64$ (d). The color map in (a),(b),(c), and (d) from blue to red indicates steady shear from low to high Pe. Solid black lines indicate G' (closed/half closed symbols) and G'' (open symbols) fits for $G'' > G'$.

frequencies ω_c for all Pe coincide. In the regime where ω_c is not measurable, the shift is performed somewhat *ad hoc* to match the full viscoelastic spectra. Figures 1(b), 1(c), and 1(d) show the scaling results for HS glasses at $\phi = 0.60$, 0.61, and 0.64. A strain rate-orthogonal frequency superposition (SROFS) is observed. In all measurements two distinct frequency regimes are separated by ω_c. For $\omega > \omega_c$ (short time scales) the elastic moduli G' superimpose for all Pe, whereas G'' data exhibit an increase with Pe (see arrow in Fig. 1). For $\omega < \omega_c$ (long time scales) the trend varies with volume fraction. In Fig. 1(b), for $\phi = 0.60$, G' and G'' superimpose well with slopes of 1.1 and 0.8, respectively. At $\phi = 0.61$, G' and G'' are closer to each other and exhibit slopes of 0.9 and 0.7, respectively [Fig. 1(c)], while at $\phi = 0.64$ [Fig. 1(d)] G' and G'' are almost identical with a slope of about 0.6.

In addition, for high Pe of the main flow and low values of ω of the orthogonal motion, the response shows some clear deviations. This is better seen in conjunction with Figs. 2(a) and 2(b), where we show for $\phi = 0.61$ the orthogonal stress amplitude, $\sigma_o^{\rm orth}$ as a function of Pe and OSR ω, respectively, and indicate liquid (open symbols) and solidlike (closed symbols) regimes. While for low Pe we mainly probe solidlike responses, as the terminal flow regime in OSR is outside of the experimental window, as Pe is increased the relaxation due to convective cage release (or shear induced out-of-cage diffusion) dominates the response, and liquidlike behavior is manifested at low OSR ω. Interestingly, at high steady shear Pe and low OSR ω we detect (beyond experimental error) a reentrant solidlike response and an increase of $\sigma_o^{\rm orth}$ with Pe [Figs. 2(a) and 2(b)]. This response, barely detectable at $\phi = 0.6$

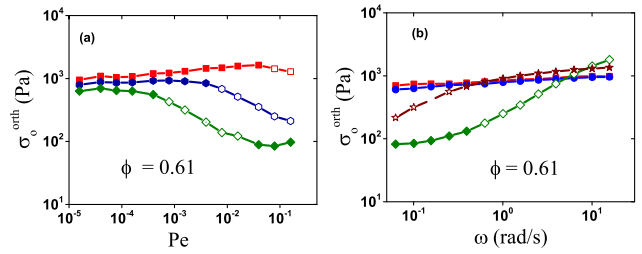

FIG. 2 (color online). (a) σ_o^{orth} vs Pe at $\omega = 0.1$ (filled diagonal), 1 (filled circle), and 10 rad/s (filled square). (b) σ_o^{orth} vs ω at Pe = 1 (filled diagonal), 0.02 (filled star), 2×10^{-4} (filled circle), and 0 (filled square) for $\phi = 0.61$. Closed symbols indicate solidlike response ($G' > G''$) and open symbols a liquidlike response ($G' < G''$).

[Fig. 1(b)], is clearly seen at $\phi = 0.61$ [Figs. 1(c), and 2(a) and 2(b)] and becomes more pronounced at the highest $\phi = 0.64$ [Fig. 1(d)].

Figure 3(a) displays the flow curves at different volume fractions (lines) together with the steady state stress reached before the superposition rheometry was performed (closed symbols). The crossover frequency ω_c is plotted for all ϕ as a function of Pe in Fig. 3(b). As seen here, ω_c exhibits a clear linear dependence with Pe over three decades for all ϕ. Interestingly, the crossover frequency is also ϕ independent, suggesting that the in-cage to out-of-cage transition time is essentially not changing within the glassy region ($\phi = 0.6$ to 0.64) and for Pe < 1 studied here.

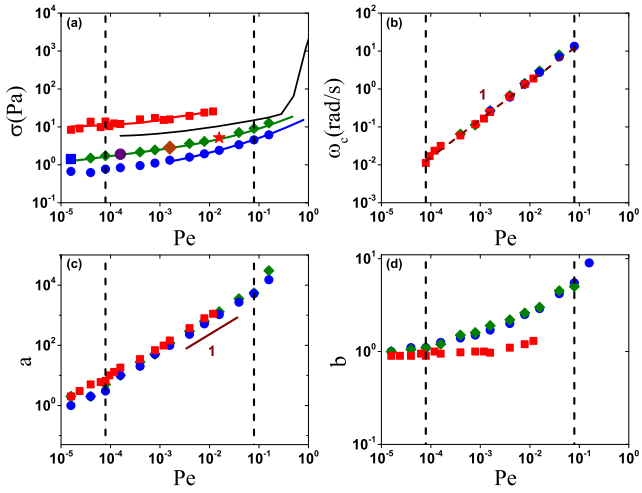

FIG. 3 (color online). (a) Flow curves superimposed with the orthogonal steady state stress at different Pe [$\phi = 0.64$ (−), $\phi = 0.61$ (−), $\phi = 0.60$ (−)]. (−) indicates the flow curve at $\phi = 0.635$ with the sudden upturn indicative of shear thickening. (b) Crossover frequency ω_c vs Pe. The horizontal shifting factor a and (d) the vertical shifting factor b used in obtaining the scaling for SROFS (Fig. 1). The vertical dashed lines indicate the frequency regime where ω_c is accessible. The symbols represent $\phi = 0.64$ (filled square), $\phi = 0.61$ (filled diagonal), and $\phi = 0.60$ (filled circle).

The horizontal and vertical scaling factors used in obtaining the scaling for SROFS (Fig. 1) are depicted in Figs. 3(c) and 3(d). In agreement with ω_c, the horizontal shift factor a rescaling time, also varies linearly with Pe [Fig. 3(c)]. In analogy with time-temperature superposition in polymers where the horizontal shifting factor relates to the temperature dependent diffusion coefficient [38], here a reflects the shear rate dependence of the transition from an in-cage to an out-of-cage motion. These findings are in agreement with the linear scaling predicted by MCT [12,39] for HS glasses, although confocal microscopy experiments with similar PMMA particles at low Pe shear have shown a power law exponent for the long time diffusion that ranges from 0.8 [23] to 1 [24].

As b is used to shift the plateau modulus it reflects the effect of shear on the in-cage free volume, similarly with the TTS where such a scaling factor represents the temperature dependence of the density [38]. Hence, b, which follows the flow curve dependence [Fig. 3(d)], is linked to the maximum limit of in-cage particle displacements prior to yielding and convective cage release. For the highest ϕ (=0.64), $b \simeq 1$ indicating the lower deformability under shear before cage release due to the smaller in-cage free volume. These observations are in line with reports of microscopic particle rearrangements in similar near-HS glasses by the technique of light scattering echo [19], where, upon increasing ϕ, irreversible rearrangements grow much sharper beyond a critical yield strain, suggesting that cages break more abruptly and the system exhibits a more brittle yielding at the microscopic level.

To further clarify the experimental results, and to rationalize deviations observed from a simple linear scaling, we resorted to BD simulations to examine shear-induced dynamics at $\phi = 0.62$. In Fig. 4(a) we plot the average mean square displacement $\langle \Delta r^2 \rangle$ from BD simulations at rest and for different Pe as a function of t/t_B. At short times we detect a drop of $\langle \Delta r^2 \rangle$ with increasing Pe [arrow in Fig. 4(a)] due to a shear-induced suppression of in-cage diffusivity first reported in Ref. [7]. When converted to viscoelastic moduli, using the generalized Stokes-Einstein (GSE) relation [40], $|G^*(\omega)| \approx k_B T/\pi a(\Delta r^2(1/\omega))\Gamma[1 + \alpha(\omega)]$ [where $\alpha(\omega) \equiv d \ln(\Delta r^2(t))/d \ln t$ at $\omega = 1/t$], such a decrease of short-time in-cage motion is manifested as an increase of G'' with Pe at high OSR ω [arrow in Fig. 4(b)]. This is in agreement with SROFS experiments (Fig. 1) and, hence, verify that the high frequency deviations in G'' are linked to such shear-induced slowing down at short-time scales, while hydrodynamic interactions (HI) are not important. The phenomenon is microscopically attributed to the buildup of structural anisotropy under shear [7], as shown in the 2D projection of the difference of the pair correlation function, $g(r)$ under shear from that at rest [Fig. 4(c)] in the velocity-gradient (xy) plane. Similarly, temperature induced structural changes in supramolecular polymers

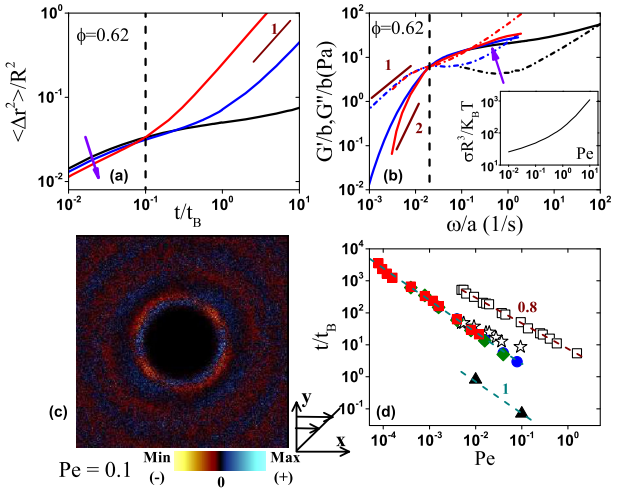

FIG. 4 (color online). (a) Mean square displacement from BD simulations for $\phi = 0.62$ when Pe $= 0$ (−), 0.01 (−), and 0.1 (−) during steady flow. (b) Shear rate orthogonal frequency superposition data deduced from BD. G' (−) and G'' (· − ·) obtained by converting MSD data of (a) for Pe $= 0$ (−), 0.01 (−), and 0.1 (−) [40]. (c) $g(r)$ in the velocity-gradient plane for Pe $= 0.1$ in steady state flow. (d) t_c/t_B calculated from ω_c for $\phi = 0.64$ (filled square), $\phi = 0.61$ (filled diagonal), and $\phi = 0.60$ (filled circle). (black filled triangle) is the t_c/t_B extracted from BD simulation for $\phi = 0.62$. (square), (star) represents t_α/t_B and t_2/t_B, respectively, for $\phi = 0.62$ calculated from Ref. [23].

were considered to be the origin of deviations at high frequencies observed in G'' when trying TTS [41].

Whereas BD simulations nicely capture and explain the experimental findings at high ω they do not agree with the experimental observations for $\omega < \omega_c$ and high steady shear Pe [as indicated by the vertical dashed lines in Fig. 4(a) and 4(b) to separate the two regimes]. At long times, $\langle \Delta r^2 \rangle$ increases linearly with time, leading to Maxwell type terminal flow with G'' and G' following power law slopes of 1 and 2 with ω, respectively [Fig. 4(b)]. Such simple flow response is markedly different from superposition rheometry experiments, where G' and G'' never acquire these terminal slopes. The discrepancy is becoming more pronounced at higher ϕ's, where the low ω regime with $G'' > G'$ is essentially absent [Fig. 1(d)] and the slopes of G' and G'' merge and decrease towards ∼0.5, indicative of a power law dependence of the relaxation spectrum. This broad spectrum found in the experiments could be caused by the presence of of hydroclusters induced by hydrodynamic interactions [3] that are absent in the BD simulations. Moreover, hydroclusters lead to a shear thickening, which was indeed detected in experiments [Fig. 3(a), for $\phi = 0.635$] at high Pe. Therefore, it seems reasonable to assume that the onset of hydrocluster formation is picked up in the superposition rheology data.

Hence, whereas there are some deviations from perfect overlap in SROFS, possibly due to hydroclusters at low ω and an effect of cage deformation on the β relaxation at high ω, most of the effect of flow can be quite nicely scaled linearly. In particular, the crossover frequency ω_c, which will govern the manner in which the system flows, scales linearly with the magnitude of the flow rate which shows that this is a convective effect. In analogy with entangled polymers where convective constraint release modifies the tube relaxation time under shear into $1/\tau = 1/t_0 + \varepsilon\dot{\gamma}$ [42,43] (t_0 is the internal relaxation time at rest and ε a constant) similar dependence had indeed been proposed for the structural relaxation in concentrated colloidal suspensions and glasses [12,20]. For a system with very long (or infinite) α relaxation, such as colloidal glasses, shear-induced flow governs the microscopic dynamics as a consequence of convective cage release of particles. ω_c ($\sim 1/\tau$) provides a measure of this relaxation time corresponding to the transition from in-cage to out-of-cage motion (as indicated by the GSE conversion), and scales linearly with Pe with $\lim_{\mathrm{Pe}\to 0}\omega_c = 0$ congruent with an infinite α relaxation time ($t_0 = t_\alpha \to \infty$) in a quiescent glass. Figure 4(d) shows the relaxation times under shear deduced from ω_c both from OSR experiments and BD simulations, the two having the same linear decrease but a difference that may be attributable to HI. For comparison, Fig. 4(d) includes the data from Ref. [23], who reported a structural relaxation time t_α and the transition to out-of-cage diffusion t_2, both, however, exhibiting clearly weaker power law dependences. The terminal relaxation time τ obtained here should be lesser than t_α and comparable to t_2 from Ref. [23]; hence, the proximity of τ to t_2 in Fig. 4(d) is reasonable, although it is still unclear why a lower power law exponent (<1) was detected in those experiments [23]. The rheological measurements do average over the entire sample, whereas the confocal experiments are limited to imaging relatively close to the wall of the flow cell.

Concluding, utilizing orthogonal superposition rheometry we are able to measure for the first time the full viscoelastic spectra of a sheared colloidal glass and obtain a scaled map of the dynamics of the system through a strain rate-orthogonal frequency superposition. Through the scaling of the crossover frequency ω_c and the shift factor b this method revealed unambiguously a linear dependence of the terminal relaxation time on the shear rate due to a convective cage release. Moreover, SROFS spectra at high frequencies provided an independent verification of the constriction of short-time in-cage motion under steady shear due to cage deformation [7], while comparison with BD simulations suggests that deviations from a terminal regime may be linked to the existence of small hydroclusters. Our findings provide valuable input to theoretical models and insights for the understanding of other soft matter or even metallic glasses under flow.

We thank Andy Schofield for particle synthesis and Nick Koumakis, Esmaeel Moghimi, and Aris Papagiannopoulos for discussions. We also acknowledge funding from EU

project "ESMI," Greek National funding through Grant THALES "Covisco" and ARISTEIA II "MicroSoft", and the Swiss National Science Foundation Grant No SNF 200021_157147. A. S. P acknowledges financial support from the DFG (Project No. SFB-TR6).

*georgp@iesl.forth.gr

[1] *Dynamical Heterogeneities in Glasses, Colloids, and Granular Media*, edited by L. Berthier, G. Biroli, J. Bouchaud, L. Cipelletti, and W. Van Saarloos (Oxford Science Publications, New York, 2011).
[2] *Soft and Fragile Matter. Nonequilibrium Dynamics Metastability and Flow*, edited by M. Cates and M. Evans (Institute of Physics Publishing, London, 2000).
[3] J. Mewis and N. J. Wagner, *Colloidal Suspension Rheology* (Cambridge Series in Chemical Engineering, Cambridge, England, 2012).
[4] F. Spaepen, Acta Metall. **25**, 407 (1977).
[5] A. Argon, Acta Metall. **27**, 47 (1979).
[6] N. Koumakis, A. B. Schofield, and G. Petekidis, Soft Matter **4**, 2008 (2008).
[7] N. Koumakis, M. Laurati, S. U. Egelhaaf, J. F. Brady, and G. Petekidis, Phys. Rev. Lett. **108**, 098303 (2012).
[8] W. van Megen and S. M. Underwood, Phys. Rev. E **49**, 4206 (1994).
[9] G. Brambilla, D. El Masri, M. Pierno, L. Berthier, L. Cipelletti, G. Petekidis, and A. B. Schofield, Phys. Rev. Lett. **102**, 085703 (2009).
[10] E. Zaccarelli, S. M. Liddle, and W. C. K. Poon, Soft Matter **11**, 324 (2015).
[11] P. Pusey, in Liquids, Freezing and the Glass Transition, *Proceedings of the Les Houches Summer School*, edited by D. L. J. P. Hansen and J. Zinn-Justin (Elsevier, Amsterdam, 1991).
[12] M. Fuchs and M. E. Cates, Faraday Discuss. **123**, 267 (2003).
[13] V. Kobelev and K. S. Schweizer, Phys. Rev. E **71**, 021401 (2005).
[14] G. Petekidis, D. Vlassopoulos, and P. N. Pusey, J. Phys. Condens. Matter **16**, S3955 (2004).
[15] R. Besseling, L. Isa, P. Ballesta, G. Petekidis, M. E. Cates, and W. C. K. Poon, Phys. Rev. Lett. **105**, 268301 (2010).
[16] P. Schall, D. A. Weitz, and F. Spaepen, Science **318**, 1895 (2007).
[17] V. Chikkadi, G. Wegdam, D. Bonn, B. Nienhuis, and P. Schall, Phys. Rev. Lett. **107**, 198303 (2011).
[18] M. Siebenburger, M. Ballauff, and T. Voigtmann, Phys. Rev. Lett. **108**, 255701 (2012).
[19] G. Petekidis, A. Moussaid, and P. N. Pusey, Phys. Rev. E **66**, 051402 (2002).
[20] K. Miyazaki, H. M. Wyss, D. A. Weitz, and D. R. Reichman, Europhys. Lett. **75**, 915 (2006).
[21] J. M. Brader, M. Siebenburger, M. Ballauff, K. Reinheimer, M. Wilhelm, S. J. Frey, F. Weysser, and M. Fuchs, Phys. Rev. E **82**, 061401 (2010).
[22] N. Koumakis, J. F. Brady, and G. Petekidis, Phys. Rev. Lett. **110**, 178301 (2013).
[23] R. Besseling, E. R. Weeks, A. B. Schofield, and W. C. K. Poon, Phys. Rev. Lett. **99**, 028301 (2007).
[24] C. Eisenmann, C. Kim, J. Mattsson, and D. A. Weitz, Phys. Rev. Lett. **104**, 035502 (2010).
[25] H. M. Wyss, K. Miyazaki, J. Mattsson, Z. Hu, D. R. Reichman, and D. A. Weitz, Phys. Rev. Lett. **98**, 238303 (2007).
[26] B. M. Erwin, S. A. Rogers, M. Cloitre, and D. Vlassopoulos, J. Rheol. **54**, 187 (2010).
[27] J. M. Simmons, J. Sci. Instrum. **43**, 887 (1966).
[28] R. I. Tanner, Trans. Soc. Rheol. **12**, 155 (1968).
[29] J. Mewis and G. Schoukens, Faraday Discuss. Chem. Soc. **65**, 58 (1978).
[30] J. Zeegers, D. van den Ende, C. Blom, E. Altena, G. Beukema, and J. Mellema, Rheol. Acta **34**, 606 (1995).
[31] J. Vermant, P. Moldenaers, J. Mewis, M. Ellis, and R. Garritano, Rev. Sci. Instrum. **68**, 4090 (1997).
[32] J. Vermant, L. Walker, P. Moldenaers, and J. Mewis, J. Non-Newtonian Fluid Mech. **79**, 173 (1998).
[33] S. Kim, J. Mewis, C. Clasen, and J. Vermant, Rheol. Acta **52**, 727 (2013).
[34] N. Koumakis, A. Pamvouxoglou, A. S. Poulos, and G. Petekidis, Soft Matter **8**, 4271 (2012).
[35] See Supplemental Material at http://link.aps.org/supplemental/10.1103/PhysRevLett.115.218301 for convective cage release in model colloidal glasses.
[36] P. Ballesta, R. Besseling, L. Isa, G. Petekidis, and W. C. K. Poon, Phys. Rev. Lett. **101**, 258301 (2008).
[37] D. R. Foss and J. F. Brady, J. Rheol. **44**, 629 (2000).
[38] M. Rubinstein and R. H. Colby, *Polymer Physics* (Oxford University Press, New York, 2003).
[39] M. Fuchs and M. E. Cates, Phys. Rev. Lett. **89**, 248304 (2002).
[40] T. G. Mason, Rheol. Acta **39**, 371 (2000).
[41] S. Seiffert and J. Sprakel, Chem. Soc. Rev. **41**, 909 (2012).
[42] G. Marrucci, J. Non-Newtonian Fluid Mech. **62**, 279 (1996).
[43] G. Ianniruberto and G. Marrucci, J. Rheol. **58**, 89 (2014).